Pulse-to-Pulse Coherent Doppler Sonar Signal Processing Techniques

ROGER LHERMITTE

University of Miami, Miami, FL 33149

ROBERT SERAFIN

National Center for Atmospheric Research,[1] Boulder, CO 80307

(Manuscript received 4 May 1984, in final form 30 August 1984)

ABSTRACT

In this paper we present and discuss techniques for the computation of the mean and spectral variance of a pulse-to-pulse coherent sonar signal, leading to the measurement of mean water velocity and turbulence. The use of an autocovariance algorithm associated with a dual-pulse repetition rate (PRF) method is recommended. The dual-PRF method allows removal of velocity ambiguities due to signal sampling and also offers a convenient means for the estimation and removal of the receiver noise which otherwise would strongly bias the spectral variance measurements. The performances of the method are illustrated by presentation and discussion of data acquired in a tidal flow.

1. Introduction

Measurement of water velocity and turbulence is currently done using *in situ* current meters and turbulence probes, possibly disturbing the flow due to their physical size. Remote sensing with Doppler sonar, which relies on the presence of very small targets tracing the flow passively, provides an attractive alternative to these methods. Indeed, useful measurements of mean water velocity have been performed using pulse Doppler sonars installed aboard research vessels and operated with either a fixed beam (Pinkel, 1979) or a three- or four-beam transducer system (Christensen, 1983).

The "single pulse" technique implemented in these sonar systems relies on the evaluation of the Doppler frequency shift within a coherent signal dwell-time that does not exceed the duration of a transmitter pulse. A pulse width of several milliseconds is required to allow a meaningful evaluation of the Doppler frequency shift, but such a signal time window is still too short to provide the frequency resolution needed to observe the spectrum of Doppler frequency shifts. The method is therefore restricted in practice to measurement of mean Doppler velocity taken as an average inside long range gates (several meters).

The basic Doppler information is nonetheless a distribution of backscattered power (Doppler spectrum) expressed as a function of the radial velocity of the targets. Observation of the Doppler spectrum mean and width can therefore constitute a useful method for measurement of water flow kinematics including turbulence. The first moment of the Doppler spectrum (mean Doppler frequency) relates to the mean flow velocity. The second central moment, or spectral variance, characterizes the spread of Doppler velocities in the scattering volume and arises from water turbulence, velocity shear and target transit time effects (Lhermitte, 1983). The interpretation of spectral moments is similar to that customary in Doppler radar methodology for studies of atmospheric motions and relies on the same assumptions about effective tracing of fluid velocity (including turbulence) by the targets. Therefore, there are incentives to resolve Doppler frequencies to much less than the spectrum width by increasing the coherent signal dwell-time well beyond that allowed by a single pulse width.

If we retain a pulse waveform, the only approach toward this goal is to evaluate the Doppler shift from the pulse-to-pulse phase change of the backscattered signal, keeping the transmitted signal phase coherent during the observation time. The phase measurements can be done independently and quasi-simultaneously at a multitude of range gates. The range gates can be very narrow since the minimum width of the transmitted pulse is now restricted only by the sonar system frequency bandwidth and signal-to-noise considerations. Therefore, in addition to providing a very high Doppler frequency resolution through the availability of a long signal dwell-time, a range resolution possibly reaching a few centimeters (compared with

[1] The National Center for Atmospheric Research is sponsored by the National Science Foundation.

a few meters for the single-pulse Doppler sonar operation) is obtained.

However, the received signal phase variation at any selected range gate is not observed *continuously* but is effectively *sampled* at the rate at which sonar pulses are transmitted (pulse repetition rate, usually referred to as PRF). Sampling of the received signal at the pulse repetition rate results in aliasing of the frequency measurements derived from the signal phase variation beyond a frequency equivalent to a maximum radial (Doppler) velocity V_{max} expressed by $\pm V_{max} = \pm f_r\lambda/4$, where f_r is the pulse repetition rate and λ the sonar wavelength. The f_r value also sets the maximum unambiguous range at which targets can be observed as $r_{max} = c/2f_r$, where c is the velocity of propagation of sonic waves underwater. Combining the above expressions, the magnitude of the problem can be represented by the classical range–velocity ambiguity function $r_{max}V_{max} = \pm c\lambda/8$.

The value of the range–velocity ambiguity function is improved by increasing the sonar wavelength. For example, for a Doppler sonar operating at 200 kHz, the ambiguity function has the value $r_{max}V_{max} = \pm 1.4 \times 10^4$ (i.e., ± 9.5 cm s^{-1} and 15 m) and extends to $\pm 1.4 \times 10^5$ (± 9.5 cm s^{-1} and 150 m) at a frequency of 20 kHz. However, the use of a lower frequency is usually associated with a reduction of the system bandwidth and therefore a decrease of the range resolution. Another consequence of lower frequency is the increased spectrum width which results from the short transit time of targets in the scattering volume. This effect can be completely ignored in the interpretation of Doppler radar data but becomes an important consideration for Doppler sonars (Lhermitte and Poor, 1983). For instance, a target moving across a beam cross section of 20 cm at a speed of 40 cm s^{-1} produces a spectrum smearing of 2 Hz. This is equivalent to a spread of radial velocity of 7.5 cm s^{-1} at 20 kHz and only 0.75 cm s^{-1} at 200 kHz. This effect does not bias mean velocity measurements, but does increase the rms error of the mean estimate (Miller and Rochwarger, 1972). However, such spectrum broadening produces an additional spectral variance that must be estimated and removed from the calculations if the measurements are to be interpreted in terms of water turbulence. Therefore, long sonar wavelengths, which provide a proportional increase of the value of the maximum unambiguous range–velocity function, also restrict the combined space–velocity resolution.

The above assessment of the range–velocity ambiguity function value must be compared with water velocities currently observed and the maximum distance at which measurements must be performed. The horizontal velocity of water ranges from less than 1 to approximately 2 m s^{-1}; its vertical velocity is much smaller so that the maximum radial (along-the-beam) velocity can be reduced by increasing the elevation angle of the sonar beams, yet allowing accurate measurements of the horizontal velocity with a multibeam system (Lhermitte and Poor, 1983). There are also numerous useful observations that can be made in shallow water (depth of a few meters to one hundred meters) such as waterways and estuaries. It was therefore decided to design and assemble a pulse-to-pulse coherent sonar system that was utilized successfully for measurements of water velocity in a tidal channel (Lhermitte, 1983).

The primary purpose of this paper is to discuss optimum methods for the evaluation of accurate Doppler spectral mean and variance estimates even if velocity ambiguities and noise are present. We will draw on signal theory and on our knowledge of the data collected using the sonar. We will explore selection and testing of multiple pulse repetition rate methods and appropriate signal processing techniques for the measurement of spectral mean and variance, such as the autocovariance (pulse-pair) time domain estimator (Woodman and Hagfors, 1969; Benham *et al.*, 1972). We will draw on past Doppler radar experience, but we will also investigate and point out the differences between Doppler sonar and radar signal processing methods.

2. Spectral moments and their estimation

A large fraction of the velocity information can be derived from the first (mean) and second (variance) spectral moments, which can be expressed by

$$\bar{f} = \int S_*(f) f df, \tag{1}$$

$$\sigma^2 = \int S_*(f)(f-\bar{f})^2 df, \tag{2}$$

where $S_*(f)$ is the Doppler spectrum normalized to unity. The higher order central moments are given by

$$\sigma^n = \int S_*(f)(f-\bar{f})^n df. \tag{3}$$

Experience acquired in the last 15 years in processing meteorological Doppler radar signals has shown that spectral moments can be more readily evaluated by implementation of time domain estimators, thereby eliminating the need for prior computation of a Fourier transform. The most widely used signal processing method, the autocovariance estimator often referred to as the "pulse-pair" estimator, is associated with minimal computational complexity and is unbiased by white noise. Moreover, autocovariance estimates of $\bar{f}$ are easily tracked through ambiguity lines and are not biased by spectrum width (Serafin and Strauch, 1978). Denenberg *et al.* (1972) presented a qualitative analysis of the performances of spectral estimators using Eqs. (2) and (3).

The pulse-pair estimator relies on the evaluation of the complex signal autocovariance $R(\tau) = C(t)C^*(t + \tau)$, where $C(t) = I(t) + iQ(t)$. Here $I(t)$ and $Q(t)$ are the in-phase and quadrature signals forming the receiver signal; $C^*(t)$ denotes the complex conjugate and $R(\tau)$ can be expressed in the following form

$$R(\tau) = R_e(\tau)e^{-i2\pi f_0\tau}. \quad (4)$$

Although $R(\tau) = a(\tau) + ib(\tau)$ is complex, the covariance amplitude $R_e(\tau)$ is an even and real quantity defined by

$$R_e(\tau) = 2\pi \int S(f - f_0)\cos(2\pi f\tau)df, \quad (5)$$

with the condition that

$$\int S(f - f_0)\sin(2\pi f\tau)df = 0. \quad (6)$$

We may define f_0 as the frequency shift needed for the Fourier transform of $S(f - f_0)$ to be real and, since $R_e(\tau)$ is real, it can be represented by

$$f_0 = \frac{\tan^{-1}[b(\tau)/a(\tau)]}{2\pi\tau}, \quad (7)$$

which applies to any spectral shape. If the spectrum is symmetrical around a mean frequency, it is obvious that f_0 is that mean since $S(f - f_0)$ becomes even, which satisfies the condition in Eq. (6).

The covariance amplitude $R_e(\tau)$ contains information on the spectrum width or variance that can be derived from the $S(f - f_0)$ spectrum. The signal autocorrelation function amplitude

$$\rho_e(\tau) = R_e(\tau)/R_e(0) \quad (8)$$

can be expressed by

$$\rho_e(\tau) = \int S_*(f - f_0)\cos(2\pi f\tau)df, \quad (9)$$

where $S_*(f - f_0)$ is the shifted spectrum normalized to its integral $\int S(f - f_0)df$. For instance, in the case of a Gaussian shape spectrum we have

$$\rho_e(\tau) = \int e^{-4\pi^2 f^2/2\sigma^2}\cos(2\pi f\tau)d\tau = e^{-2(\pi\sigma\tau)^2}. \quad (10)$$

For a given τ_0, this leads to the evaluation of σ^2 from

$$\sigma^2 = -\frac{\ln\rho_e(\tau_0)}{2\pi^2\tau_0^2}. \quad (11)$$

Although Eq. (11) applies rigorously to a Gaussian shape spectrum only, $\rho_e(\tau)$ can be easily evaluated from (9) for symmetric spectra expressed by simple integrable functions. We have performed such computations for the spectral shapes shown in Fig. 1, which are: exponential, triangular, square, triangle–bimodal and the extreme case of bimodality represented by two narrow spectral regions located on both sides of the zero frequency. All of these spectra

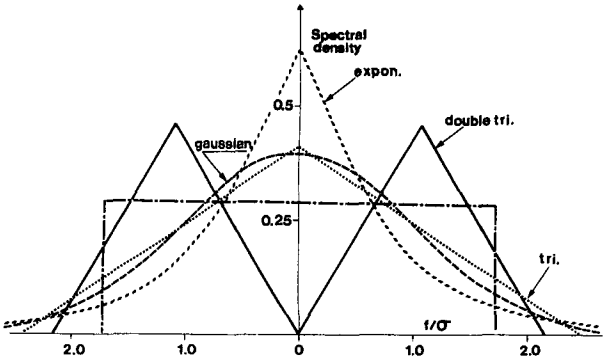

FIG. 1. Spectral models used in the computations. The spectral density indicated is normalized to the area under the spectrum. The frequency is normalized to the spectrum standard deviation.

are symmetrical about their mean which, for our variance computations, is set to be 0. Although they are associated with a small bias of the spectral mean estimate, asymmetrical spectra have not been considered.

Some of the results of the $\rho_e(\tau)$ computations are shown in Fig. 2 as a function of the nondimensional quantity $\sigma\tau$. All of the autocorrelation functions tested become identical when $\sigma\tau$ approaches zero, a condition that holds in practice for $\sigma\tau < 0.1$, for all spectral shapes tested with the exception of the exponential spectrum. For larger values of $\sigma\tau$, the autocorrelation functions associated with non-Gaussian spectra have lesser values than those evaluated for Gaussian spectra, except for the case of an exponential shape spectrum.

In the case of the pulse-pair operation, we must recall that the sample time interval τ_0 is also the time lag. The $\pm 1/(2\tau_0)$ Nyquist boundaries will thus replace the $\pm\infty$ boundaries in integrals such as (9). Spectra with width exceeding the Nyquist frequency interval will be folded; recovery of the spectral shape will be impossible and frequency domain estimates of σ will be biased. To prevent folding, the total spectrum width should not extend beyond these boundaries. This sets a maximum value of $\sigma\tau_0$, which can be derived from the relationship between spectrum maximum width and variance. For example, this maximum value of $\sigma\tau_0$ is 0.2–0.16 for a Gaussian spectrum, approximately 0.2 for an exponential spectrum, 0.204 for a triangular spectrum and 0.5 for a bimodal spectrum composed of two narrow spectral regions on both sides of the zero frequency. Figure 3 shows the systematic error arising from applying Eq. (11) to spectral shapes other than Gaussian. The results are shown as the ratio σ_g/σ, between the estimate σ_g, based on the Gaussian shape assumption, and the true σ value. This ratio is expressed as a function of $\sigma\tau$. If we consider a limit of $\sigma\tau < 0.16$ (Gaussian spectrum), the discrepancy does not exceed 8%. Incidentally, Pasarelli *et al.* (1984) have shown that the

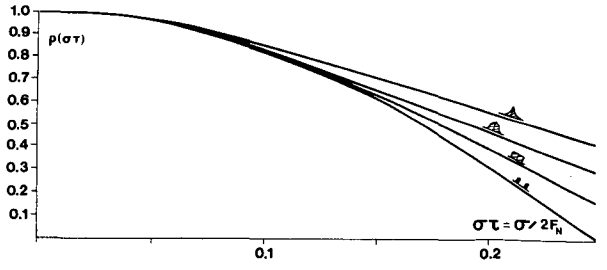

FIG. 2. Real term $\rho(\tau)$ of the autocorrelation function for the different spectral shapes indicated.

autocorrelation function is invariant in the presence of folding, and therefore pulse-pair estimates of the autocovariance function are theoretically not affected by spectrum width.

The ratio σ_g/σ is related to the actual spectrum flatness represented by the kurtosis coefficient $K = M_4/(M_2)^2$, where M_2 and M_4 are the second and fourth spectral moments. The relationship between K and the bias on σ induced by a different spectral shape is shown in Fig. 4. If K is less than its value for a Gaussian spectrum ($K = 3$), the procedure from (11) overestimates σ. Measurements of K from an extension of the pulse-pair algorithm (Pasarelli and Siggia, 1981) should, in principle, provide a method for correcting the bias in the estimate of σ based solely on pulse-pair algorithms. However, although it is found theoretically that K is within reasonable limits (between 1 and 6) for the spectra investigated, our experience indicates that its experimental value can sometimes greatly exceed these limits. This may render the use of K as a correction factor doubtful.

3. Differences between pulse-pair and frequency domain estimators

It is generally agreed that the pulse-pair technique is an accurate method for the measurement of mean Doppler frequency, as only spectrum skewness produces a small bias of the estimate. However, there is no clear understanding of the effectiveness of that estimator in measuring spectral variance accurately. The theoretical derivations above are adequate, but they ignore the presence of noise in experimental data and other problems that limit the value and interpretation of the measurements. Since Doppler sonar data can be obtained continuously and repeatedly in a tidal flow, they offer a unique opportunity to investigate the advantages and limitations of the two estimators. This will be pursued in the following sections of this paper but, before proceeding any further, we should examine a fundamental difference between the evaluation of variance from the spectral second moment and that derived from the pulse-pair algorithm.

The velocity spectrum estimated from a Fourier transform of the sonar signal is a statistical entity

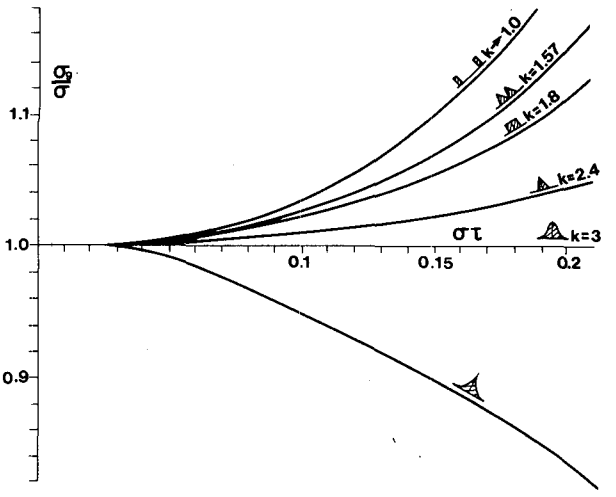

FIG. 3. Ratio of the estimate of variance, assuming a Gaussian-shaped spectrum σ_g^2, to the true spectral variance σ^2 for the spectral shapes indicated.

including all velocity components occurring during the total observation time. This property also applies to spectra that are continuously added, since all velocity components in any of the individual spectra will contribute to the overall velocity statistics. This includes the effect of time fluctuations of Doppler velocity experienced by the targets and larger scale eddies traveling through the scattering volume. The spectral variance will thus increase continuously with time as new scales become part of the statistics, and its final value will include all of those scales that have contributed to the spectra. However, once the variance of a spectrum has been evaluated, application of the

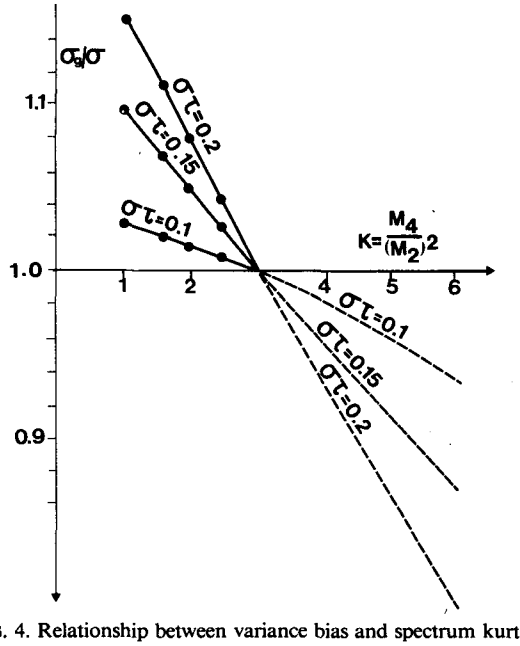

FIG. 4. Relationship between variance bias and spectrum kurtosis.

same procedure to other spectra observed later will not bring any variance contribution arising from variations with respect to the frequency content of previous spectra.

If we examine carefully the principle of the pulse-pair estimator operation, we discover that this estimator evaluates the variance of a *snapshot* of the velocity distribution relating only to the motion of targets during the short pulse-to-pulse time interval. Therefore, it is referred to as an "instantaneous" velocity mean. Repeating the measurements involving successive pulse-pair samples leads to the evaluation of an average value of this short-term variance that does not include velocity fluctuations at time scales exceeding the short pulse-pair time interval. The method is thus insensitive to variations of the instantaneous velocity mean, such as that produced by eddies translating through the sonar pulse volume, occurring over times exceeding the pulse-pair time interval. This may be considered to be an advantage of the pulse-pair technique since the lower wavenumber (larger scale) involved in the variance measurements is unambiguously related to pulse volume size only.

The difference between the results given by the two estimators processing the same signal can be used to separate these variance contributions—i.e., instantaneous velocity variance from the pulse-pair and longer term variance involving fluctuations of the mean. Note that the linear mean is not biased by this effect and also that the longer scale information can be restored by analyzing the short-term fluctuations of the pulse-pair derived mean.

4. Influence of noise on the estimation of variance

Processing and analysis of large amounts of Doppler sonar data have revealed that, even with a large signal-to-receiver noise power ratio, a substantial spectral noise background is always present. The occurrence of this spectral noise may severely limit the interpretation of results in terms of the spectral variance evaluated using the estimators discussed in this paper. The origin of this noise, which is always significant (spectral signal-to-noise power ratio rarely exceeds 10 to 17 dB), is not clearly established. There are suspected contributions such as loss of signal coherence during underwater propagation going to and coming from the targets and backscattering by the water which may be associated with a very wide spectrum. If the noise is produced by mechanisms induced by sonar-signal propagation and scattering, it is a fundamental part of the backscattered signal and cannot be eliminated or even reduced through improvement of the sonar system. It is therefore necessary to investigate methods to evaluate and then remove the contribution to variance arising from the noise. The presence of such white noise in the data does not bias the estimate of the mean Doppler velocity and, because of our large data sample size, does not increase the variance of that estimate appreciably compared with its natural variability. Nevertheless, the noise can introduce a significant (sometimes overwhelming) bias of the spectrum variance estimate if not properly accounted for. Thus, as an approach to evaluating and removing the noise, we will investigate the amount of variance increase produced by this noise and the response of the estimators to that effect.

Let us assume a uniform white noise spectrum S_n, extending to the Nyquist boundaries $\pm f_1 = \pm 1/(2\tau)$, and a signal spectrum of unknown shape S_s with a total width sufficiently small so that there is negligible folding of the signal spectrum at the $\pm f_1$ boundaries. Both spectra are defined only within the Nyquist interval $\pm f_1$ or, in the case of symmetric spectra, between 0 and f_1.

The variance of the composite spectrum is

$$\sigma_{sn}^2 = \frac{\int S_s f^2 df + \int S_n f^2 df}{\int S_s df + \int S_n df}. \tag{12}$$

If we introduce the noise-to-signal power ratio

$$\alpha = \frac{P_n}{P_s} = \frac{\int S_n df}{\int S_s df}, \tag{13}$$

and substitute this expression in (12), we have

$$\sigma_{sn}^2 = \frac{\sigma_s^2 + \alpha\sigma_n^2}{1 + \alpha}, \tag{14}$$

which is the variance effectively evaluated from (2) for signal and noise.

The term σ_{sn}^2 varies from σ_s^2 (no noise) to σ_n^2 (no signal). If we recall that $\sigma_n^2 = f_1^2/3$ (variance of white noise defined between $\pm f_1 = \pm 1/2\tau$), we can express the ratio between the variance of the signal and noise σ_{sn}^2 and the variance of the signal alone σ_s^2 by

$$\frac{\sigma_{sn}^2}{\sigma_s^2} = \frac{1 + \alpha/(12\sigma_s^2\tau^2)}{1 + \alpha}. \tag{15}$$

The contribution to spectral variance arising from the noise-to-signal power ratio α is reduced as $\sigma\tau$ increases; i.e., if the signal spectrum extends to the greatest fraction of the Nyquist frequency interval $\pm f_1$ compatible with the condition of negligible spectrum folding.

Indeed, the evaluation of σ_s^2 based on Eq. (15) shows that for $\alpha = 30$ dB and $\sigma_s\tau > 0.05$ the bias is less than 1%, increasing to 4% for $\sigma_s\tau = 0.025$ and 15% for $\sigma_s\tau = 0.0125$. For a 20 dB noise-to-signal ratio, the variance excess is less than 1% for $\sigma_s\tau = 0.166$ (maximum spectrum width for a Gaussian

spectrum), 10% for $\sigma_s\tau = 0.05$ and a whopping 67% for $\sigma_s\tau = 0.025$. A 10 dB value for α requires $\sigma_s\tau > 0.1$ to make the measurements meaningful if no noise correction is attempted. Recall, however, that a decrease of $\sigma_s\tau$ reduces the influence of spectral shape on the value of the autocorrelation function, but this is negligible compared with the enhancement of the noise effect on spectral variance associated with small $\sigma_s\tau$ values.

Assuming again a white noise extending to the Nyquist boundaries $\pm f_1$, for which $\sigma_n^2 = f_1^2/3$, the relative contribution to variance due to signal alone and the contribution due to noise can be separated if two independent spectral variance estimates σ_1^2 and σ_2^2 are evaluated using two different lags τ_1 and τ_2. The method is similar to that proposed by Srivastava *et al.* (1979) but it applies to any values of the τ_1 and τ_2 lags and any signal spectral shape. The only restriction is that the noise must be white regardless of the sonar pulse repetition rate. Assuming that both signal and noise are stationary processes, and using Eq. (14) for the expression of σ_1^2 and σ_2^2 we have

$$\sigma_1^2 = \frac{\sigma_s^2 + \alpha f_1^2/3}{1 + \alpha}, \tag{16a}$$

$$\sigma_2^2 = \frac{\sigma_s^2 + \alpha f_2^2/3}{1 + \alpha}. \tag{16b}$$

Solving (16a) and (16b) for α, we have

$$\alpha = \frac{\sigma_1^2 - \sigma_2^2}{\sigma_2^2 - \sigma_1^2 + (f_1^2 - f_2^2)/3}, \tag{17a}$$

and solving for σ_s^2, we have

$$\sigma_s^2 = \frac{\sigma_2^2 f_1^2 - \sigma_1^2 f_2^2}{3(\sigma_2^2 - \sigma_1^2) + f_1^2 - f_2^2}. \tag{17b}$$

The autocovariance estimator operates on a different principle and does not necessarily yield the same variance estimate in the presence of noise as predicted by Eq. (15). The response of the pulse-pair algorithm to the presence of noise can be evaluated using the expression of the autocorrelation function, $R_{sn}(\tau)$, for signal and noise. We have

$$R_{sn}(\tau) = P_s\rho_{e[s]}(\tau)e^{-i\omega_0\tau} + P_n\delta(\tau), \tag{18a}$$

where $\delta(\tau)$ is the Kronecker-delta function defined by $\delta(\tau) = 1$ for $\tau = 0$ and by $\delta(\tau) = 0$ for $\tau \neq 0$. We have

$$\rho_{sn}(\tau) = \frac{R_{sn}(\tau)}{P_s + P_n} = \frac{\rho_s(\tau)e^{-i\omega_0\tau} + \alpha\delta(\tau)}{1 + \alpha}, \tag{18b}$$

with α defined in Eq. (4). Then,

$$\rho_{e[sn]}(\tau_0) = \frac{\rho_{e[s]}(\tau_0)}{1 + \alpha}. \tag{19}$$

Equation (19) is a general result for the amplitude of the autocorrelation function when the noise is white.

Let us assume a signal with known spectrum shape and variance for which the relationship between $\rho_s(\tau)$ and $\sigma\tau$ is known explicitly. Applying that relationship to ρ_{sn} yields a variance estimate σ_{sn}^2, which can be compared to the signal variance σ_s^2. In the case of a Gaussian spectrum $\rho(\tau)$ is given by

$$\rho_{e[s]}(\tau) = e^{-2\pi^2\sigma_s^2\tau^2}, \tag{20}$$

so that σ_{sn}^2/σ_s^2 is given by the expression

$$\frac{\sigma_{sn}^2}{\sigma_s^2} = 1 + \frac{\ln(1 + \alpha)}{2(\pi\sigma_s\tau)^2}. \tag{21}$$

The other spectral shapes considered earlier produce almost identical results for small $\sigma\tau$ values.

The results of these computations are shown in the form of the ratio σ_{sn}/σ_s, as a function of $\sigma\tau$ in Fig. 5. The notation for this quantity is the same as that evaluated previously for spectral variance from (15) (which is also presented in the same graph), but now applies to pulse-pair results. One sees that the pulse-pair variance bias is slightly less than that resulting from the use of the frequency domain estimator except for very high noise-to-signal ratio conditions. Note that the noise variance is limited to $f_1^2/3$ but that the pulse-air estimate solution for noise alone has no boundary ($\sigma = \infty$ if $\rho_e = 0$).

The same method proposed above (also discussed earlier by Srivastava *et al.*, 1979), which involves two independent evaluations of the autocorrelation function (ρ_1 and ρ_2) using two different time lags or pulse repetition periods (τ_1 and τ_2), offers a means to separate the contribution of signal and noise in the pulse-pair results. Applying this technique to a Gaussian-shaped signal spectrum, and assuming again a white noise extending to the $\pm f_1$ boundaries, we have

$$\rho_1 = e^{(-2\pi^2\sigma_s^2\tau_1^2)}/(1 + \alpha), \tag{22}$$

$$\rho_2 = e^{(-2\pi^2\sigma_s^2\tau_2^2)}/(1 + \alpha), \tag{23}$$

from which we evaluate

$$\sigma_s^2 = \frac{\ln(\rho_1/\rho_2)}{2\pi^2(\tau_2^2 - \tau_1^2)}, \tag{24}$$

$$\alpha = [e^{(-2\pi^2\sigma_s^2\tau_1^2)} - \rho_1]/\rho_1. \tag{25}$$

Thus, σ_s^2 and α can be derived effectively from the above expressions. This requires a dual-pulse repetition rate (PRF) scheme, but can be implemented, as suggested by Srivastava *et al.* (1979), by using a single PRF and generating the second lag by skipping every other sample ($\tau_2 = 2\tau_1$).

5. Data acquisition and processing

The data presented in this paper were acquired using a sonar system that was described in detail by Lhermitte (1983). The methodology for the interpretation of water mean velocity and turbulence from the Doppler sonar data, including the separation of variance and covariance terms in a multibeam

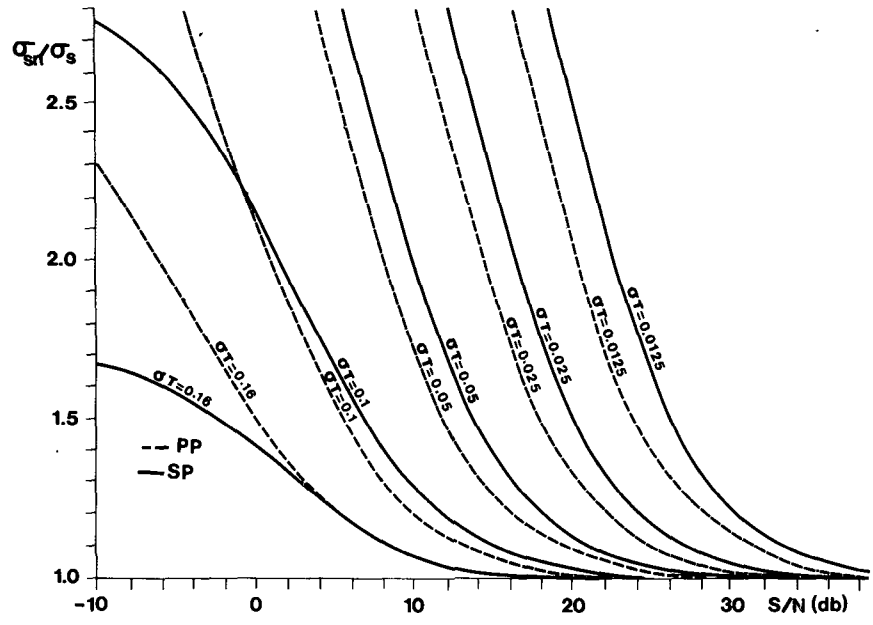

FIG. 5. Ratio of the signal-to-noise variance σ_{sn}^2 to the signal variance σ_s^2, as a function of the signal-to-noise power ratio for several $\sigma\tau$ values. The results are shown for both the spectral variance (SP) and the pulse-pair (PP) methods.

method, was also discussed extensively (Lhermitte, 1983; Lhermitte and Poor, 1983). This does not have to be repeated here.

The sonar system is composed of a conventional pulse transmitter and a receiver followed by a phase detector circuit producing the "in-phase" I and "quadrature" Q outputs, which are effectively the real and imaginary parts of a complex signal. This complex signal is necessary to provide the sign of the Doppler frequency shift, i.e., to remove the folding at zero frequency inherent in a real (single) signal (Lhermitte, 1983). For best results, the outputs of the phase detector are range-integrated during one pulse width and sampled and digitized at the end of each integration bin ("range gate"). The receiver signal is thus sampled and digitized at range gates spaced by a sonar pulse width. The I and Q samples are then stored temporarily in a random access memory for further on-line processing by a Fourier transform unit that produces 128 spectra, each composed of 128 frequency points, in approximately 2 seconds. A separate random access memory provides means for accumulating spectra over time periods possibly exceeding several minutes before they are stored on magnetic tape.

In addition to the Fourier transform operation, the sonar electronics performs on-line evaluation of the autocovariance partial products, namely: I_1I_2, Q_1Q_2, I_1Q_2, I_2Q_1, I_1I_1, Q_1Q_1 where subscripts 1 and 2 denote successive signal samples separated by the time interval τ_0. Each of the partial product terms is recorded using a 16-bit format, which retains almost full data accuracy. Both the Fourier transform and the evaluation of autocovariance terms are performed systematically at the 128 range gates.

After recording, the data are processed by a computer that evaluates the first four spectral moments from the recorded spectra. Before this evaluation is performed, the DC spectral component is systematically removed and replaced by the interpolated value between the spectral density at two spectral lines on both sides of the zero frequency. This procedure, which affects only the zero frequency spectral line, does not modify appreciably the results of the evaluation of spectral moments and was introduced in the computations to overcome the effect of a possible DC drift of the I and Q signals. This DC offset was later reduced considerably through careful adjustments of the I and Q signal means to prevent the occurrence of a bias in the pulse-pair estimates. The only possible spurious contribution to zero frequency may arise from the unlikely presence of fixed target returns "seen" through sonar transducer sidelobes.

The computer program used for the evaluation of the spectral moments includes the option of a threshold (Hildebrand and Sekhon, 1974) set arbitrarily 10 dB below the spectrum peak. The purpose behind the use of a threshold is to remove the baseline noise in the spectrum in an effort to eliminate this contribution to the estimated spectral variance. A 10 dB threshold is roughly equivalent to signal equal noise for a spectrum bandwidth ten times less than the Nyquist boundaries. The estimate of the variance obtained using the threshold is corrected for the lack of signal spectral information below the threshold by assuming a Gaussian-shaped spectrum.

The pulse-pair partial products are used to compute the mean Doppler frequency from

$$\bar{f} = \frac{\tan^{-1}[(I_1I_2 + Q_1Q_2)/(Q_1I_2 - Q_2I_1)]}{2\pi\tau_0}. \quad (26)$$

The amplitude of the autocorrelation function $\rho_e(\tau)$ is evaluated from

$$\rho(\tau) = \frac{[(I_1I_2 + Q_1Q_2)^2 + (I_1Q_2 - I_2Q_1)^2]^{1/2}}{I_1^2 + Q_1^2}. \quad (27)$$

The variance estimate is computed according to (11), i.e., assuming a Gaussian-shaped spectrum and a noise-free signal.

The computer program includes graphical presentation of the data in various forms such as raw spectra and slant range profiles of spectral mean and variance evaluated using either the frequency domain (10 dB threshold and no threshold) estimator or the pulse-pair algorithm. Additional programs perform computation of u, v and w, and evaluation of variance and covariance terms from the five-beam data (Lhermitte, 1983); they also include the noise correction algorithms based on dual-PRF techniques discussed previously. Because of their representativeness regarding the very large quantity of data produced by the system, the program also includes means for statistical plots between any of the variables computed.

The data presented here were collected using a five-beam transducer platform resting on a tidal channel bottom (see Fig. 6). Each of these transducers produces a 3° (3 dB points) sonar beam and can be selected independently of the others. One beam is directed vertically with a pointing accuracy better than 0.03°. The other four beams are tilted (elevation angle 75°) and pointed in the N–S–E–W directions with the north–south pair essentially aligned with the longitudinal flow. The Doppler sonar was sometimes operated with two sequentially selected pulse repetition rates. The beams are switched successively in an automatically repeated sequence possibly combined with dual PRF operation. The pulse width (and the range gate spacing) is 3 cm. Because of its excellent pointing accuracy,the vertically pointing beam provides the most accurate and reliable spectral variance data that are also immune from contamination by sidelobe effects (Lhermitte and Poor, 1983).

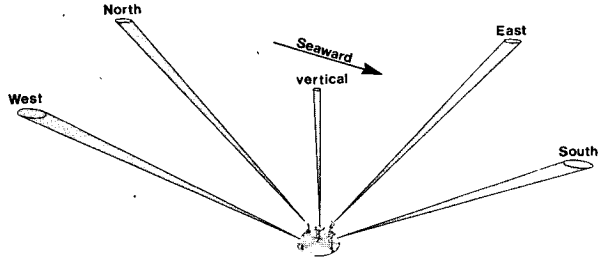

FIG. 6. Configuration of the five beams that are part of the transducer assembly. The center beam is directed vertically; the elevation angle of the tilted beams is 75°.

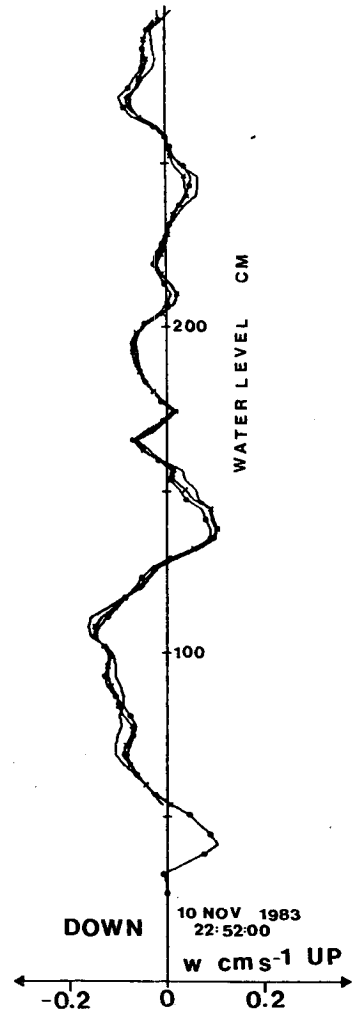

FIG. 7. Mean vertical velocity evaluated from the spectral mean 10 dB threshold (solid line), no threshold (line with plus signs) and the Pulse-Pair algorithms (dotted line). The water level indicated is upward from the channel bottom.

In the following sections we present and analyze some of the data acquired by the system in an effort to compare these experimental results with the previous theoretical discussion.

6. Mean Doppler results

Figure 7 shows an example of the mean vertical velocity profiles evaluated from the three estimators, namely, pulse-pair algorithm (PP), no-threshold spectral mean (NT) and 10 dB threshold spectral mean. Note the low values of velocity (less than 0.2 cm s^{-1}). The PP Doppler means and the NT spectral mean estimates agree within 0.02 cm s^{-1}. The 10 dB threshold estimates (T) deviate slightly more (less than 0.04 cm s^{-1}). Figure 8 shows the same data for the radial velocity observed with the north beam (75° elevation angle). There is, again, excellent agreement

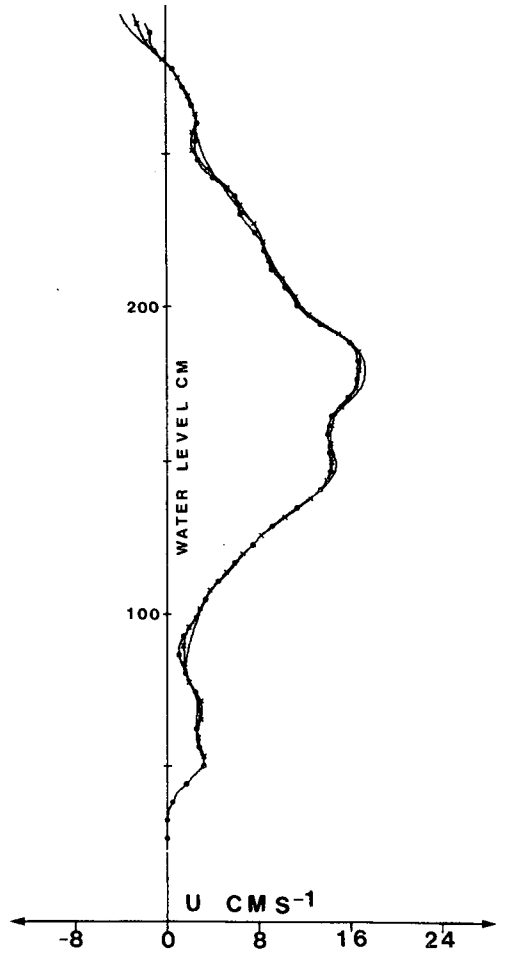

FIG. 8. As in Fig. 7, but for a tilted beam along the flow, during a flood regime.

between NT and PP estimates, but also small deviations of the T estimate from the other two profiles.

The statistical plots (T versus PP, NT versus PP and T versus NT) for all beams at all water depths for data observed during 90 min in a flood regime are shown in Fig. 9a–c. These examples, although involving only 2500 data points, are representative of results obtained with other and more extensive data sets. As shown in Fig. 9a, the best least-squares fit between two different velocity mean estimates (slope of 0.9854 and correlation of 0.9997) is observed for NT versus PP. The other least-squares fits shown in Figs. 9b and c (slope of 0.9701 and correlation of 0.9991 for T versus PP, and slope of 0.9846 and correlation of 0.9995 for T versus NT) exhibit slightly worse results. The good agreement of NT and PP estimates indicates that the bias of the PP estimate due to possible spectrum skewness is negligible. The introduction of the 10 dB threshold used to remove the effect of spectral noise produces a small bias and a slight loss of correlation. This could possibly indicate noise rejection. However, the noise is not expected to bias the mean velocity estimate, but only to increase its variance slightly, and the use of a threshold is not recommended. The PP method, therefore, emerges as a very reliable processing technique, and there is no need to perform a Fourier transform to evaluate the Doppler mean velocity. The only justification for frequency domain processing is the filtering of undesirable frequency components such as a fixed target return. However, backscattering from the water surface seen through the transducer sidelobes is the only spurious Doppler component we have identified, and the spectral width associated with it makes its removal through filtering difficult.

Figures 10a and b show slant range mean velocity profiles observed with pulse repetition rates associated with aliasing boundaries of ± 9.2 and ± 2.3 cm s^{-1}, respectively. One sees again that there is good agreement between the three mean Doppler estimators. There is, however, a better matching of the lower PRF data.

These results show that high-order velocity ambiguities can, indeed, be resolved using dual (or multiple) PRF schemes. However, as indicated by Fig. 10c, which shows on the same graph two profiles acquired at slightly different times, there is significant time variability of the mean water velocity over short time periods. Such fluctuations of water velocity are the main factors limiting the highest velocity ambiguity order that can be resolved. This problem is alleviated by interleaving pulse repetition periods so that the two data sets are essentially derived from the same signal dwell-time period for both PRFs. Note that this procedure is easily implemented with PP but not with Fourier transforms.

Figure 11 shows a statistical plot of w versus u for velocity data acquired at all depths between the channel bottom and the water surface, collected during six complete tidal cycles; u is the true horizontal velocity evaluated from the four N–S–E–W profiles (Lhermitte, 1983), and w is the velocity observed by use of the vertically pointing beam. Both u and w are mean velocities evaluated for a total signal time on the order of 1 min. One sees that the variability of w and the range of u are high, but there is very little correlation between the two. This indicates an extremely small tilt of the vertically pointing beam which, if significant, would produce an easily detected u versus w correlation, since w is much smaller than u. A least-squares fit of the data indicates that, indeed, the correlation between u and w is very small and can be explained by a 0.03° tilt of the vertically pointing beam axis. Incidentally, the mean of all the w data points evaluated over the six complete tidal cycles is approximately 0.001 cm s^{-1} downward, which is compatible with the settling velocities of small particulates. The preceding results induce confidence in the quality of the Doppler sonar velocity measurements and the ability of the targets to trace mean water velocity.

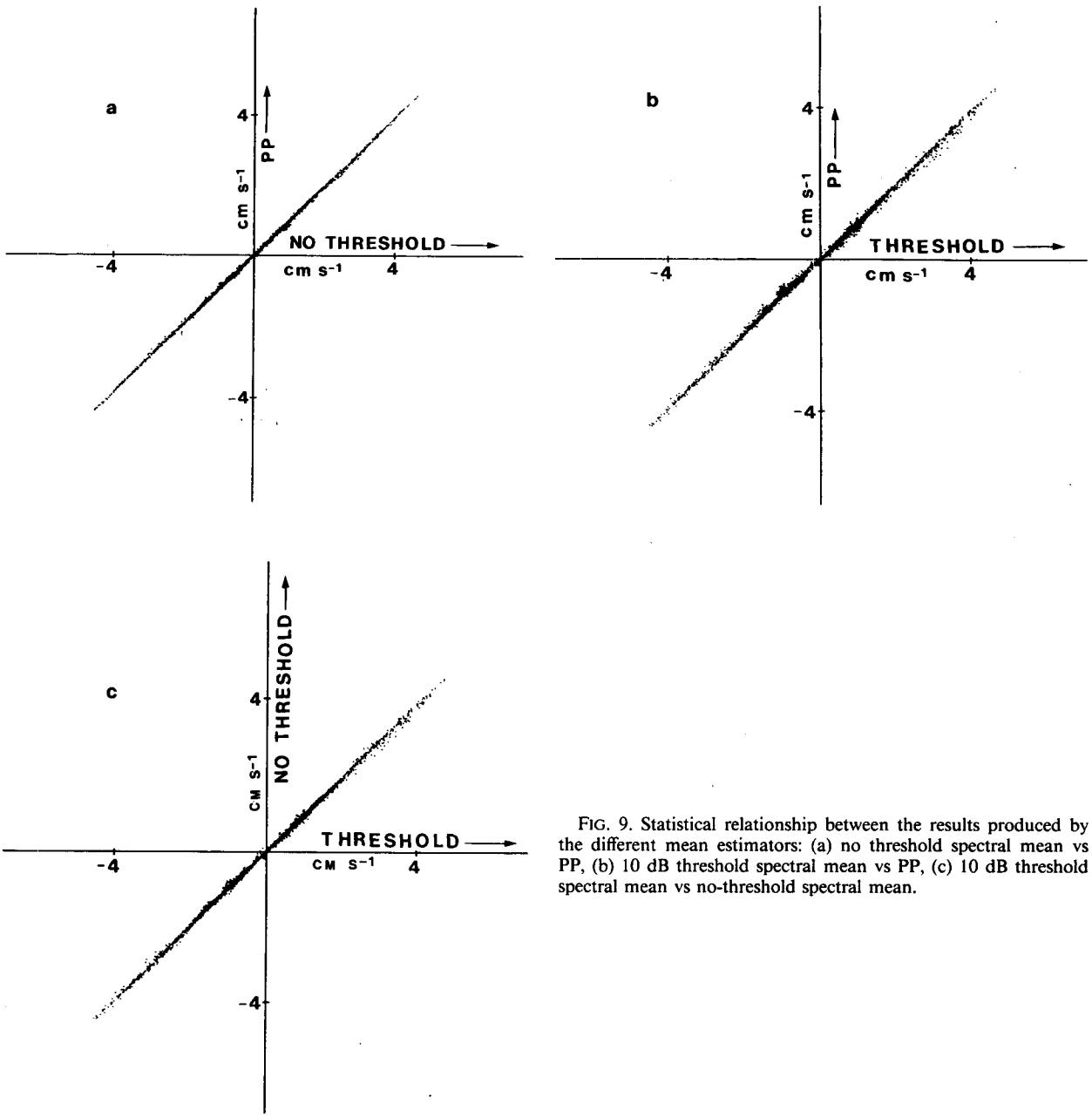

FIG. 9. Statistical relationship between the results produced by the different mean estimators: (a) no threshold spectral mean vs PP, (b) 10 dB threshold spectral mean vs PP, (c) 10 dB threshold spectral mean vs no-threshold spectral mean.

7. Variance measurements and their interpretation

Before we discuss the association between spectral variance and the velocity distribution inside a pulse volume, let us consider examples of the short-term spectral mean variance.

Figure 11 indicates that the variance of the vertical velocity mean w, evaluated in a time interval of approximately 1 min, reaches ~ 0.01 cm^2 s^{-2} for an horizontal flow velocity of 10 cm s^{-1}. Note that the 1 min integration time used in the evaluation of the mean relates to eddy scales greater than approximately 5 m (8–10 cm s^{-1} horizontal velocity), which are certainly strongly horizontally elongated.

By comparison, Fig. 12 shows a statistical plot of vertical velocity short-term spectral variance σ_w^2 versus longitudinal flow velocity. One sees that, on average, σ_w^2 increases with u. Also, σ_w^2 has a nonzero value for $u = 0$, because, in a tidal flow, still water is only a short transition from ebb to flood regimes, and the water turbulence does not have time to dissipate. We also see that at $u = 10$ cm s^{-1}, for instance, the value of σ_w^2 varies from 0.02 to more than 1 cm^2 s^{-2} which is considerably greater than the short-term mean variance values presented previously.

These results indicate that small-scale spectral variance, which is confined to a few centimeter scales extending down to the turbulence dissipation sub-

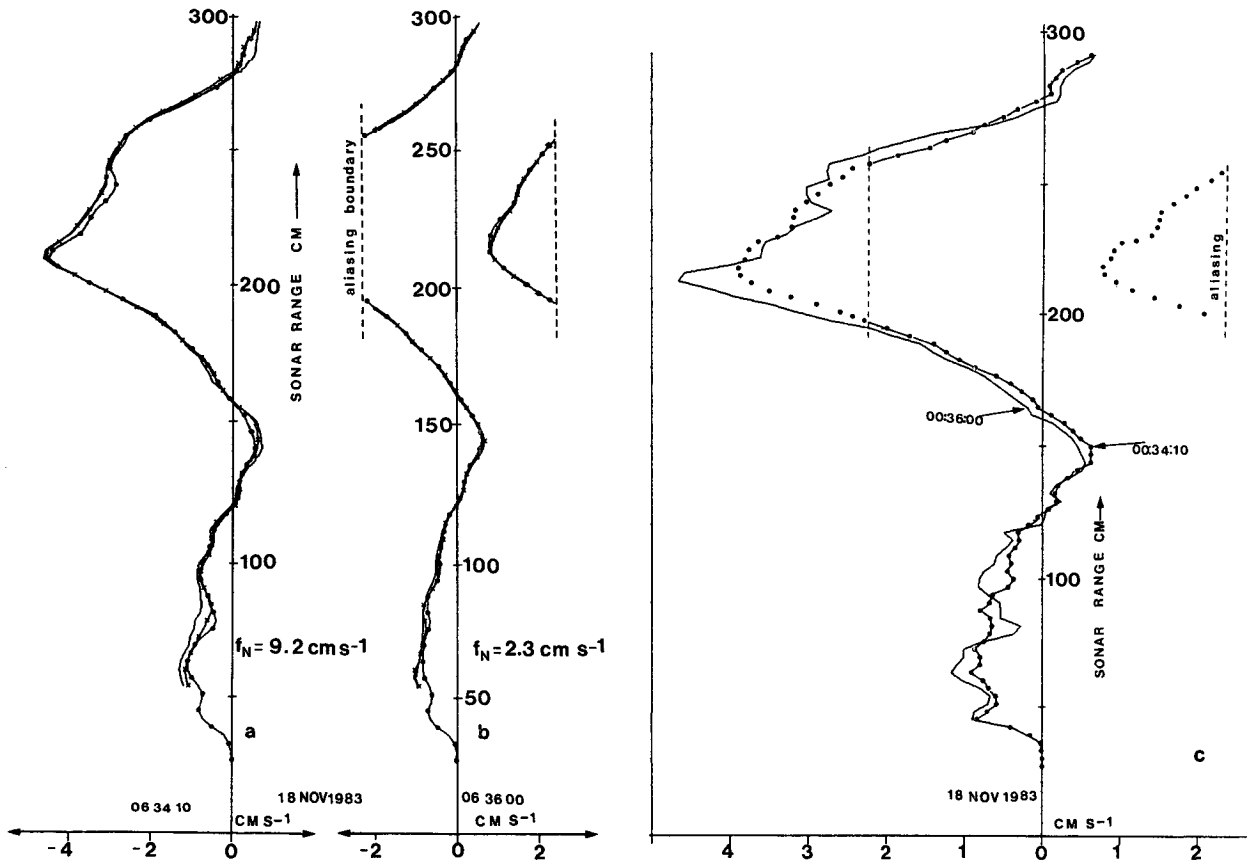

FIG. 10. Effect of frequency aliasing: (a) relates to a 9.2 cm s^{-1} Nyquist boundary, (b) relates to a 2.3 cm s^{-1} Nyquist boundary; time difference is 2 min. Note that the agreement between PP and spectral mean is on average better for lower Nyquist boundaries; (c) shows the two profiles on the same graph.

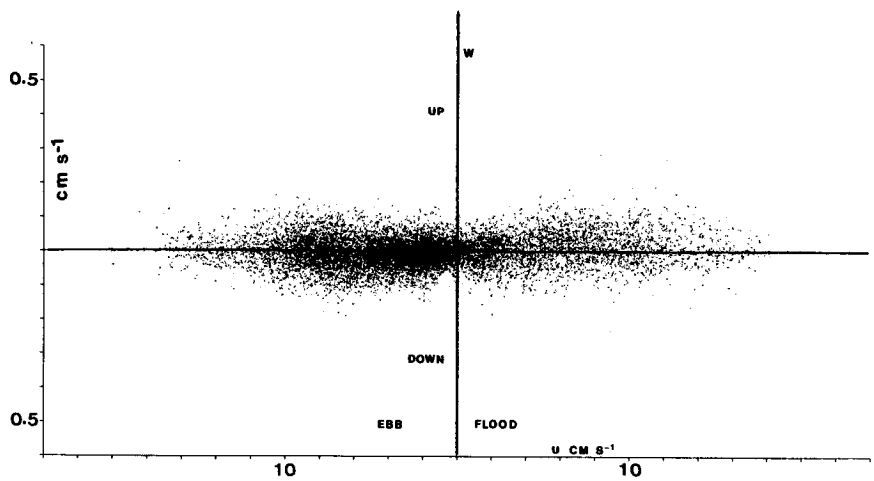

FIG. 11. Statistical relationship between w and u for all the velocity observations at all depths during six complete tidal cycles. Each of the data points is evaluated in approximately 1 min. Although w exhibits substantial fluctuations, these are not correlated with u. A least-squares fit indicates a very small slope of the w vs u relationship, consistent with a tilt of the beam axis of less than 0.03°.

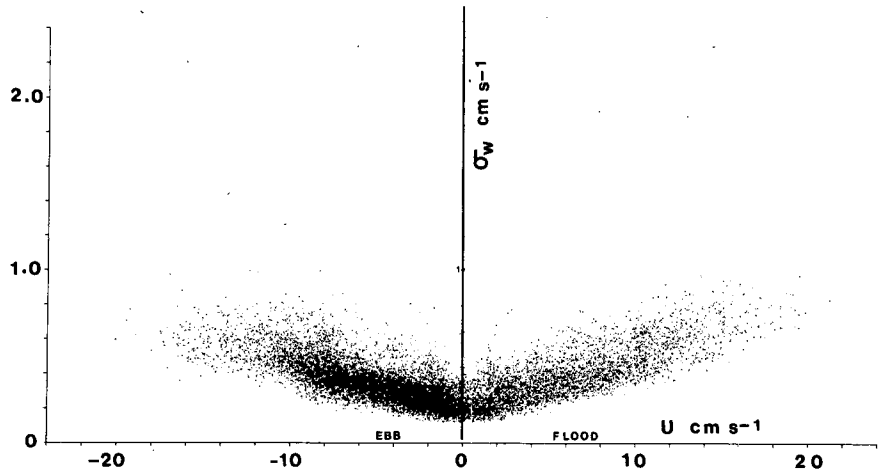

FIG. 12: Statistical relationship between σ_w (square root of the vertical velocity variance) and the longitudinal velocity u. This well-defined relationship provides incentives for the measurements of σ_w as the basic tool for the understanding of water turbulence and its relation to longitudinal flow and stability parameters.

range, accounts for a large fraction of the velocity variance. As an additional example of the usefulness of short-term velocity variance measurements, Fig. 13 shows vertical profiles of mean horizontal velocity together with spectral variance profiles observed with the vertically pointing beam σ_w^2 and with the tilted

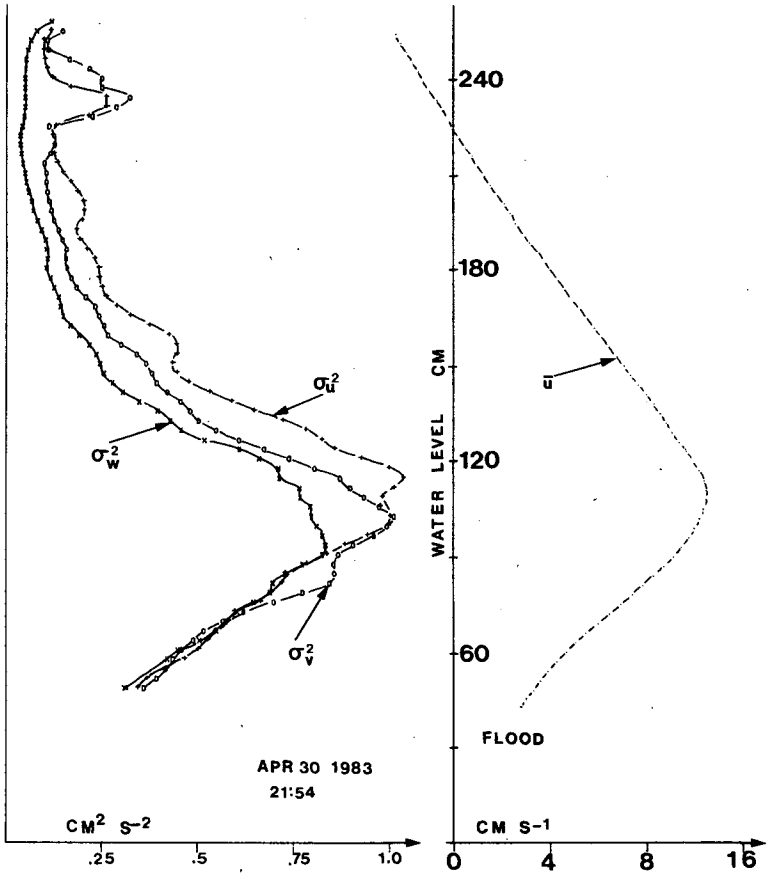

FIG. 13. Relationship between vertical velocity variance for the vertical and tilted beams and the longitudinal flow.

beams. The variance components observed with the tilted beams (σ_u^2 along the flow, σ_v^2 across the flow) are taken along the slant range and, therefore, include both the horizontal and vertical velocity variances. These data were collected during a flood regime. In the bottom of the profile below the velocity maximum, the three variance components have the same values within the random uncertainties of the measurements, indicating the isotropic nature of the turbulence below the profile nose. Above the velocity nose σ_w^2 becomes smaller than σ_u^2, which indicates horizontal elongation of the turbulent eddies.

8. Influence of noise

The above examples are presented to provide strong incentives for accurate measurements of small-scale spectral variance. However, corrections must be applied to the Doppler sonar variance observations before they can be interpreted in terms of water turbulence alone. These problems have been considered in earlier papers (Lhermitte, 1983; Lhermitte and Poor, 1983). The presence and influence of spectral noise further complicates the interpretation of the variance, and this problem should be carefully

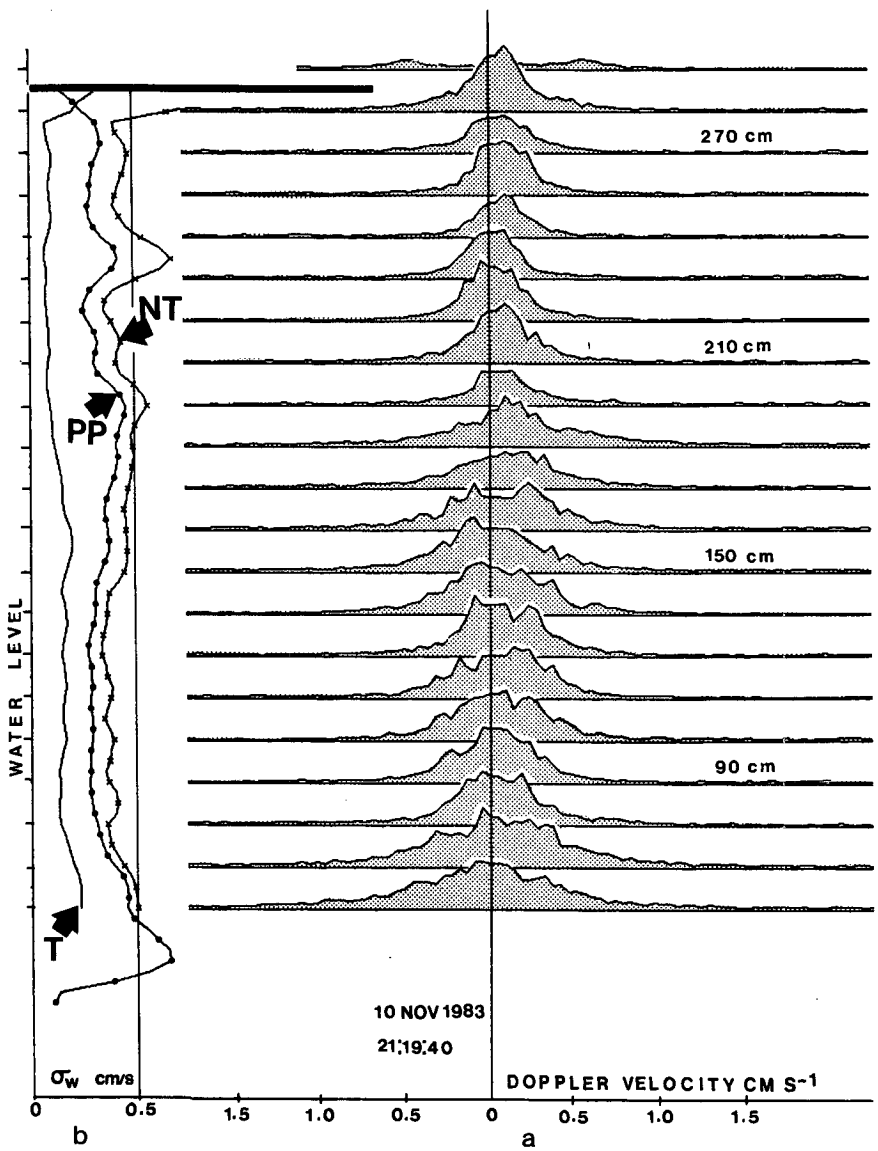

FIG. 14. (a) Raw spectra (ordinate in each spectrum proportional to the square root of spectral density) observed with the vertically pointed beam. The velocity scale is indicated; the Nyquist boundary is 2.3 cm s^{-1}. Note the bimodal spectrum beyond the water surface which indicates an amplitude modulation of the signal associated with reflection at the water surface. (b) Vertical profiles of variance evaluated from: 1) spectral variance with a 10 dB threshold (T), 2) spectral variance without threshold (NT) and 3) pulse-pair algorithm (PP).

addressed. Therefore, this section of the paper is devoted to testing the theoretical methods for noise evaluation and removal proposed earlier, using experimental results: i.e., actual Doppler spectra observed with the Doppler sonar.

Before proceeding further we will show in Fig. 14a a typical example of raw Doppler spectra. The data were acquired with the vertically pointing beam just after still water in a preflood tidal regime. The spectra are systematically processed by the on-line Fourier transform unit at range gates spaced by 3 cm in slant range. However, only the spectra acquired at 12 cm depth intervals are shown. In order to allow an easier perception of their dynamic range in the graph, the spectra are represented by the square root of spectral power density as a function of Doppler frequency or radial velocity. The spectra are well defined, but detailed inspection reveals that the signal-to-noise ratio does not exceed 25 dB, independent of signal level. Since the receiver signal is carefully filtered to reject frequency components outside of the Nyquist frequency, this indicates that the noise must be part of the received signal itself, perhaps due to a mechanism of backscattering by the clear water as suggested earlier.

Figure 14b shows the profiles of vertical velocity spectral variance evaluated using the estimators presented and discussed previously. In this case NT refers to no-threshold spectral variance; T, 10 dB threshold spectral variance; and PP, variance evaluated using the pulse-pair algorithm Eq. (11). The spectrum observed beyond the water surface (water level of 294 cm from bottom) becomes bimodal, which may be attributed to a modulation of the sonic wave reflection at the water surface. If the water surface is rougher and more chaotic, a white spectrum associated with the loss of phase coherence experienced by the sonic wave after its reflection by the interface is usually observed.

There are significant differences among the three profiles. The estimate derived from a 10 dB threshold spectral variance computation provides the smallest variance values. However, the use of a 10 dB threshold is arbitrary and tends to underestimate the variance appreciably, as compared with a subjective estimate of that variance made by estimating spectral width graphically. The NT method definitely overestimates σ^2 with respect to that derived from spectral shape and width, and this is certainly due to the influence of noise. The PP estimate provides a variance estimate closer to graphical estimation of spectral width, but still overestimates σ^2. Before we discuss methods for improving the spectral variance estimates derived from the PP algorithm, let us consider the influence of observation time on the results.

Figure 15a shows the variance profiles acquired with a signal dwell-time of 105 s; Fig. 15b shows the same profiles observed 2 min later, but evaluated with a much reduced (15 s) dwell-time. As discussed before, the estimate of variance from the pulse-pair algorithm does not include scales greater than the scattering volume dimension and is not expected to be influenced by an increase of the total signal dwell-time unless the small-scale variance itself changes. The variance derived from spectrum width should, however, include all scales associated with the increased dwell-time. The fact that no appreciable increase of the spectral variance estimate with a larger signal dwell-time is seen in Figs. 15a and b, supports the statement made earlier that a large fraction of the turbulent kinetic energy is at scales smaller than the scattering volume dimensions. Note, however, that these results are concerned with variance of the vertical component of velocity and would be different if related to horizontal velocity components.

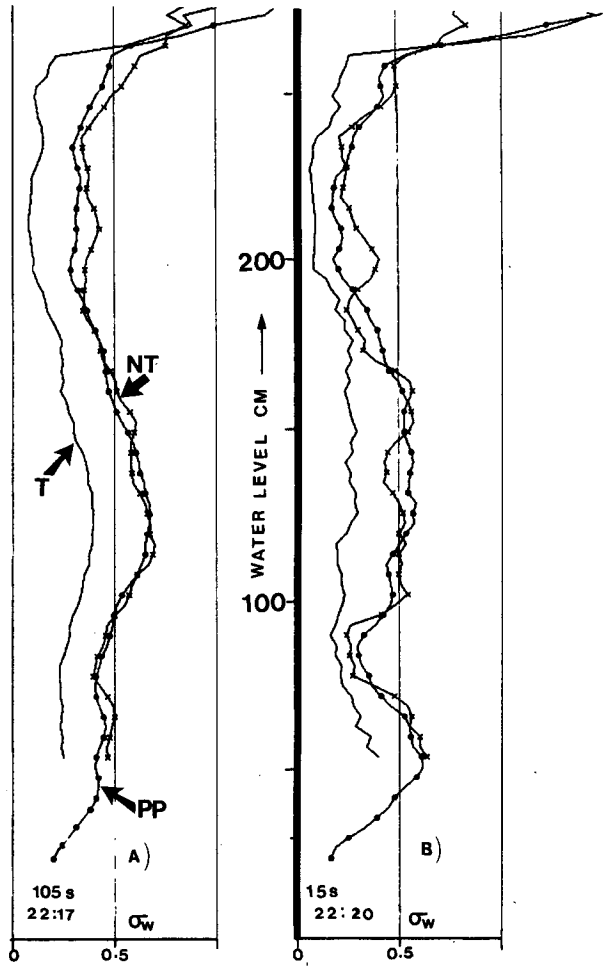

FIG. 15. Vertical profiles of spectrum variance for different signal dwell-times, 105 and 15 s. Even with that considerable difference between dwell-times, the pulse-pair profiles are very similar. The longer dwell-time, however, provides smoother profiles.

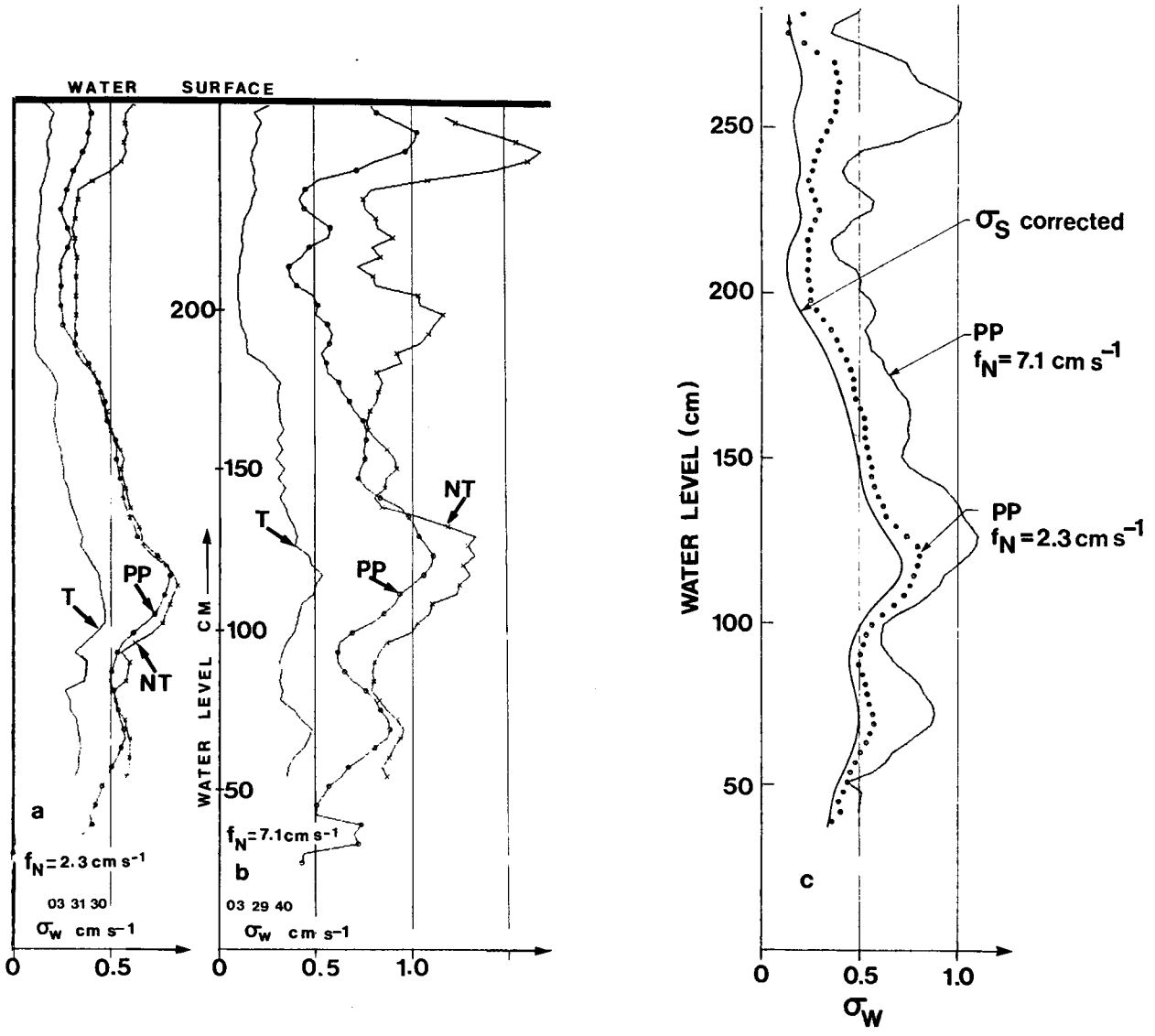

FIG. 16. Vertical profiles obtained with the three variance estimators for (a) 2.3 and (b) 7.1 cm s^{-1} Nyquist boundaries; (c) shows the PP profiles and the variance corrected for noise according to (24) (see text).

Figures 16a and b show the variance profiles obtained with two different pulse repetition rates associated with 2.3 and 7.1 cm s^{-1} Nyquist boundaries. The data were taken 2 min apart, but there was little change of the variance profiles during this time, as indicated by the stability of the 10 dB threshold variance estimates. However, the change of PRF produces a drastic difference in the variance estimates from both the NT and PP estimates. This was predicted earlier from Eqs. (15) and (19), which express the influence of noise on spectral variance. The noise contribution is, indeed, a function of the ratio of spectrum width to Nyquist interval, which is expected to change with the PRF for the same spectral width. Note that the PP estimate is less sensitive to that effect and, also, usually provides much smoother profiles.

If we assume that the noise is white, which is confirmed by inspection of the spectra, we can apply Eq. (24), discussed previously, in an effort to derive the signal spectra variance σ_s^2 alone, from the values of σ^2 obtained with the two PRFs. The results are shown in Fig. 16c together with the two PP-derived variances. Note that the values obtained through the use of the noise correction methods discussed above agree well with variance measurements derived from estimates of spectrum shape and width, which, even if they are obtained subjectively from a graphical

outline of the spectrum, provide a better perception of the noise baseline level. Therefore, the dual PRF/pulse-pair appears to be an appropriate technique for the measurement of variance in the presence of noise.

9. Conclusion

The measurement of velocity mean from Doppler sonar data using the PP algorithm is an optimum method with respect to both effectiveness and simplicity. It is our perception, based upon the analysis of experimental data, that velocity aliasing ambiguities reaching more than five orders can be resolved. However, this procedure requires interleaving the pulse repetition periods to alleviate the detrimental effect of time variability of the velocity mean which would otherwise be the main limiting factor in resolving high-order ambiguities.

There are strong incentives for measuring spectral variance and relating these measurements to water turbulence. However, since the data always exhibit the presence of substantial spectral noise (signal-to-noise = a few decibels to at most 25 dB), the noise contribution to spectral variance must be estimated and removed. Inspection of each of the spectra presented graphically may be the most reliable method to separate signal and noise contributions to variance. However, it is not practical for systematic processing of large amounts of Doppler data. The introduction of a threshold before the computation of spectral moments is too arbitrary and has a tendency to underestimate spectral variance. Therefore, the PP method, if used in conjunction with an interleaved dual-PRP scheme, in addition to being objective, simple and straightforward, appears to be the best available method. Research is underway to estimate the best choice of PRFs to optimize the method.

Acknowledgments. The computer programs were designed and assembled by Mr. Henry Poor with great professional skill. This research was performed under National Science Foundation Grant OCE 8214018, monitored by Mr. Larry Clark.

REFERENCES

Christensen, J. L., 1983: A new acoustic Doppler current profiler. *Sea Technol.*, **24,** 10–13.

Denenberg, J. M., R. J. Serafin and L. C. Peach, 1972: Uncertainties in coherent measurement of the mean frequency and variance of the Doppler spectrum for meteorological echoes. *15th Radar Meteorology Conf.*, Champaign-Urbana, Amer. Meteor. Soc., 216–221.

Groginsky, H. L., A. Soltes, G. Works and F. C. Benham, 1972: Pulse pair estimation of Doppler spectrum parameters. Final Report. Raytheon Company, Wayland, MA. 158 pp. [NTIS AD 744094.]

Hildebrand, P. H., and R. S. Sekhon, 1974: Objective determination of noise level in Doppler spectra. *J. Appl. Meteor.*, **13,** 808–811.

Lhermitte, R., 1981: Observations of water flow with high resolution Doppler sonar. *Geophys. Res. Lett.*, **8,** 155–158.

——, 1983: Doppler sonar observation of tidal flow. *J. Geophys. Res.*, **88,** 725–742.

——, and H. Poor, 1983: Multi-beam Doppler sonar observations. *Geophys. Res. Lett.*, **10,** 717–720.

Miller, K. S., and M. M. Rochwarger, 1972: A variance approach to spectral moment estimation. *IEEE Trans. Inform. Theory,* **IT-18,** 588–596.

Pasarelli, R. E., and A. D. Siggia, 1981: The autocorrelation function and spectral moments: Geometric and asymptotic interpretation. *20th Conf. Radar Meteorology,* Boston, Amer. Meteor. Soc., 301–307.

——, R. J. Serafin and R. Strauch, 1984: Effects of aliasing on spectral moment estimates derived from the complete autocorrelation function. *J. Climate Appl. Meteor.*, **23,** 848–849.

Pinkel, R., 1979: Observations of nonlinear motion in the open sea using a range-gated Doppler sonar. *J. Phys. Oceanogr.*, **9,** 675–680.

Serafin, R. J., and R. Strauch, 1978: Radar signal processing. *Air Quality Meteorology and Atmospheric Ozone,* Morris and Barras, Eds., Amer. Soc. for Testing and Material, Philadelphia, PA, 159–182.

Srivastava, R. C., A. R. Jameson and P. H. Hildebrand, 1979: Time computation of mean and variance of Doppler spectra. *J. Appl. Meteor.*, **18,** 189–194.

Woodman, R. F., and T. Hagfors, 1969: Methods for the measurements of vertical ionospheric motions near the magnetic equator by incoherent scattering. *J. Geophys. Space Phys.*, **75,** 1205–1212.

Zrnić, D. S., 1977: Spectral moment estimates from correlated pulse pair. *IEEE Trans. Aerosp. Electron.*, **AES-13,** 334–354.